Dephasingless Plasma Wakefield Photon Acceleration

R. Sandberg* and A. G. R. Thomas†
Gérard Mourou Center for Ultrafast Optical Sciences, University of Michigan, Ann Arbor, MI 48109, USA
(Dated: January 3, 2024)

The paper [R.T. Sandberg and A.G.R. Thomas, Phys. Rev. Lett. 130, 10.1103/PhysRevLett.130.085001 (2023)] proposed a scheme to generate ultrashort, high energy pulses of XUV photons though dephasingless photon acceleration in a beam driven plasma wakefield. An ultrashort laser pulse is placed in the plasma wake behind a relativistic electron bunch such that it experiences a comoving negative density gradient and therefore shifts up in frequency. Using a tapered density profile provides phase-matching between driver and witness pulses. In this paper, we give the details of the wakefield solutions and phase matching conditions used to generate the phase-matching density profile. The short, high-density, and weak driver limits are considered. We show, explicitly, the numerical algorithm used to calculate the density profiles.

I. INTRODUCTION

The many applications of bright, coherent XUV light have motivated substantial interest in source development, such as the construction of XUV wavelength Free Electron Lasers such as FLASH [1] as well as nonlinear frequency mixing [2], high harmonic generation [3], relativistic flying mirrors [4–6], and XUV lasing [7], to name a few. Another method for generating short wavelengths is 'photon acceleration' [8, 9].

From the linear, unmagnetized plasma dispersion relation $\omega^2 = k^2c^2 + \omega_p^2$, where $\omega_p^2 = e^2n/m_e\varepsilon_0$ for a plasma of number density n, it can be seen that if we identify a localized electromagnetic energy wavepacket with central frequency ω as a 'quasi-photon', and consider its quasi-photon energy and momentum $E = \hbar\omega$ and $\vec{p} = \hbar\vec{k}$, when propagating in the background plasma it will gain an effective "mass" $\hbar\omega_p/c^2$. The wavepacket group velocity is $\vec{v}_g = \vec{k}/\omega$ and hence if its frequency is up-shifted, the dispersion relation implies that the 'quasi-photon' will travel at a higher velocity, i.e. it is accelerated. In the presence of co-propagating density gradients, the 'quasi-photons' experience local frequency shifts due to spatiotemporal variations in the phase velocity [10], and are therefore accelerated. The resulting quasi-photon phase space trajectories in plasma wakefields are similar to those of leptons [11].

Photon acceleration can arise as a result of plasma wakefields [8], ionization fronts [12, 13] and even using metamaterials [14]. Photon acceleration was measured in ionization front [15] and laser wakefield acceleration experiments [16, 17]. Recent results include cascaded sequences of localized ionizations [18], resulting in large frequency shifts and the use of plasma wakes to downshift radiation to very long wavelengths [19]. Limits to photon acceleration in plasma wakefields in the linear [20] and nonlinear regimes [21, 22] were previously studied, identifying dephasing of the photon beam with respect to the accelerating refractive index gradient as placing a ceiling on the frequency shift. Dephasing occurs when the difference between the phase velocity of the wake and the high-frequency photon pulse results in it slipping out of the accelerating refractive index gradient. A recent scheme for overcoming this restriction using an ionization front is dephasingless frequency shift using a 'flying focus,' a combination of a chirped laser pulse and an achromatic lens for spatiotemporal shaping of a laser pulse [23]. The flying focus was also used to mitigate the analogous process of electron beam dephasing in a plasma wakefield [24], in addition to related spatiotemporally structured focusing schemes [25, 26].

Another method for mitigating dephasing, in the context of electron acceleration is the use of tapered plasma density ramps [27–30]. By having a non-uniform density, the plasma wavelength varies along the propagation length, which allows for locking the accelerating phase with the particle beam. Tapered density ramps were previously suggested as a way of increasing the frequency shifts in photon acceleration [8, 20]. In our recent paper [31], we showed that by using a relativistic-charged-particle-beam driven 'photon-accelerator' with a tapered density ramp, dephasing could be mitigated and large frequency shifts were possible, limited only by the available driver energy. With a beam driver we found that the appropriate density profile is a down-ramp rather than the up-ramp considered in previous studies of the laser driven case. We refer to this as the dephasingless plasma wakefield photon acceleration (dePWPA). In one dimensional ab-initio relativistic electromagnetic particle-in-cell simulations we demonstrated a more than 50 times frequency shift.

In this paper, we expand on the details of the analytic model used for the results of Ref. [31], including the derivation of the beam driven wakefield solution and the phase matching condition and validate approximations in the short driver limit. We also explicitly give the algorithm used to solve the equations to calculate the tapered density profile needed to mitigate dephasing. In section

* rsandberg@lbl.gov, presently at Lawrence Berkeley National Laboratory.
† agrt@umich.edu.

II, we review the frequency shift and phase matching condition required for dePWPA given first in our paper [31] for completeness. In section III, we develop the solution for the wakefield given behind an arbitrary density and length beam driver pulse; the one-dimensional wake solutions for a wakefield driven by a 'top-hat' profile beam were first developed by Rosenzweig [32] for the weak driver beam case, $n_d/n < \frac{1}{2}$, where n_d is the drive beam density. We extend this model to solutions for arbitrary drive beam density $n_d/n \geq \frac{1}{2}$. In section IV we show the method for solving the dephasing condition, including the computational algorithm (the actual Python code used to calculate the density maps used in Ref. [31] is also included as supplemental material). In section V, we study the approximations to the solutions in the short, high-density (SHD) and weak driver limits. In particular, we show that as the plasma density drops for the dephasingless scheme, the driver approaches the SHD limit and so the SHD limit is valid initially for a large fraction of initial beam parameters and asymptotically for all beam parameters. Finally, we conclude in section VI.

II. DEPHASINGLESS PHOTON ACCELERATION

A. Frequency shifts in the presence of a density gradient

A laser pulse that experiences a co-moving plasma density gradient will be upshifted in frequency. From eikonal solutions to the wave equation, well known ray-tracing solutions can be used for the temporal variation in the light [9, 33] to relate it to the density gradients generated in a wakefield. For a given dispersion relation D, the frequency ω and wavenumber k_z of an optical mode propagating in the z direction satisfy the following relations:

$$\begin{aligned} dz/d\tau = \partial D/\partial k_z, \quad dk_z/d\tau = -\partial D/\partial z\ , \\ dt/d\tau = \partial D/\partial \omega, \quad d\omega/d\tau = \partial D/\partial t\ . \end{aligned} \tag{1}$$

The optical mode will vary with distance propagated as

$$\begin{aligned} \frac{d\omega}{dz} &= \frac{d\omega/d\tau}{dz/d\tau} \\ &= \frac{\partial D/\partial t}{\partial D/\partial k_z}\ . \end{aligned} \tag{2}$$

We assume that the laser pulse is propagating in a wakefield generated by a relativistic driver (either a relativistic particle beam or second laser pulse) propagating at velocity $v_d(z)$ and therefore change coordinates from (x, y, z, t) to $(x, y, z, \zeta = t - \int_0^z dz'/v_d(z'))$ [28]. The change in the frequency can, therefore, be expressed as

$$\frac{d\omega}{dz} = \frac{\partial D/\partial \zeta}{\partial D/\partial k_z}\ . \tag{3}$$

For example, for linear plasma dispersion, $D = \omega^2 - \omega_p^2/\gamma - k^2c^2$, and assuming that ions are immobile and the variations in the plasma density with respect to ζ are much larger than the variations in ω and k,

$$\frac{d\omega}{dz} \simeq \frac{1}{2k_z c^2}\frac{\partial(\omega_p^2/\gamma)}{\partial \zeta}\ . \tag{4}$$

Note that the γ factor in the linear dispersion relation is to allow for relativistically streaming electrons rather than, e.g. oscillations in the laser field, and therefore this dispersion relation is considered exact for a weak laser pulse.

B. Matching condition to mitigate dephasing

For positive frequency shift, the laser pulse must be at a phase in the wake where the density is gradient is positive with respect to the coordinate ζ. However, the laser centroid moves at the group velocity of the laser pulse and so as the laser pulse shifts in frequency, its group velocity increases and the pulse will change position in the wake. To mitigate dephasing of the photon pulse, we use a tapered density profile (similar to that proposed for mitigating dephasing in electron acceleration [28, 30, 34, 35]) to continuously increase the plasma wavelength and keep the laser pulse experiencing a positive plasma density gradient.

Here, we derive the phase-matching condition for a one-dimensional (1d) nonlinear plasma wake, which we find is also accurate to describe the three-dimensional case for a broad driver ($k_p\sigma_r \gg 1$), where $k_p = \omega_p/c$ and σ_r is the is the root-mean-square beam radius. Under the assumption that $d\log(n)/dz \ll k_p(z)$ for all z, i.e. the plasma density gradients are long compared to the wake period scale, to lowest order the wake may be assumed to follow the uniform plasma solution with local density $n(z)$. Hence, we write the perturbed density of the wake $n_w(\zeta; z)$ as a function of ζ parameterized by z, i.e. by the local density $n(z)$.

For convenience, we choose the point where the density perturbation in the wake $\delta n(\zeta; z) \equiv n_w(\zeta; z) - n(z) = 0$ within the region of positive density gradient, hereby labelled as ζ_δ, as the location of the reference density gradient we are trying to track. This is not the maximum density gradient except in the linear regime, but the maximum is in general only slightly behind ζ_δ, and using ζ_δ greatly simplifies the analysis. It can be shown that the maximum refractive index gradient occurs where the electric field of the wake is zero, which is close to where the density perturbation goes to zero. It can also be shown that the refractive index gradient is equal to the density gradient at the point where $\delta n = 0$ for a 1D wake.

To keep the pulse experiencing the greatest possible frequency shift, we require $\zeta_{\text{centroid}} = \zeta_\delta$ for all times, where ζ_{centroid} denotes the center of the witness laser pulse. Expressed in differential form, we have

$$\frac{d\zeta_{\text{centroid}}}{dz} = \frac{d\zeta_\delta}{dz} \,, \tag{5}$$

which may be written as

$$\frac{1}{v_{\text{centroid}}} - \frac{1}{v_d} = \frac{d\zeta_d}{dn}\frac{dn}{dz} \,. \tag{6}$$

For an ultrarelativistic particle beam driver, we make the approximation $v_d \to c$. Assuming that the laser pulse moves at the linear group velocity and the plasma is underdense, $\omega_p^2/\omega^2 \ll 1$, we obtain an equation relating the z profile of the plasma number density to the variation in the wake position of the zero density perturbation ζ_δ with plasma density,

$$\frac{dn}{dz} \simeq \frac{1}{2c}\frac{\omega_p^2}{\omega^2}\left[\frac{d\zeta_\delta}{dn}\right]^{-1} \,. \tag{7}$$

Note that $\gamma(\zeta_\delta) = 1$, where the density perturbation is zero.

The phase matching condition in equation (7) and the frequency shift relation in equation (4) together are a coupled pair of differential equations for the plasma density profile that will give phase matched photon acceleration as well as the predicted frequency shift given the phase matched density profile. To close them, it remains to determine the dependence of the quantities $\left.\frac{\partial(\omega_p^2/\gamma)}{\partial\zeta}\right|_{\zeta_\delta}$ and $\frac{d\zeta_\delta}{dn}$ on n and ω.

III. DESCRIPTION OF THE WAKE BEHIND THE DRIVER

In this section, the position ζ_δ in the wake where $\delta n = 0$ and there is a positive density gradient is obtained, along with the density gradient at that position. We derive these quantities using a 1D model for the wakefield, which we find is accurate to describe the three-dimensional case in the broad driver ($k_p\sigma_r \gg 1$) approximation, where $k_p = \omega_p/c$ and σ_r is the root-mean-square beam radius. The wake behind the driver is modeled with the 1D Akhiezer-Polovin (AP) [36] relativistic wave. This is an undriven plasma wave with a given amplitude γ_m and phase velocity $\beta_w = v_p/c$; in this work the wave phase velocity is assumed to be ultrarelativistic, $\beta_w \to 1$.

For clarity, we express the equations in normalized units, with all plasma densities $n \to n/n_0$ where n_0 is a reference plasma density. Also $\omega_p \to \omega_p/\omega_{p0}$, $\omega \to \omega/\omega_{p0}$, $p \to p/m_e c$, etc., where $\omega_{p0}^2 = e^2 n_0/m_e\varepsilon_0$, $E \to eE/mc\omega_{p0}$, etc.

The Lagrangian form of the plasma equations describing the AP wave is used here to develop a solution parameterized in terms of a periodic coordinate φ as derived by Infeld and Rowland in [37] (particularly, the expression of the Infeld-Rowland-Akhiezer-Polovin wave derived in Verma et al. [38, 39].) With the parameterization of the wake behind the driver, the position of zero density perturbation, ζ_δ, and the plasma density gradient there, $\left.\frac{\partial(\omega_p^2/\gamma)}{\partial\zeta}\right|_{\zeta_\delta}$, are found as functions of the wake parameters φ_{st} and amplitude γ_m defining the wake behind the driver. Then, the dependence of the starting phase φ_{st} on the wake within the driver is found, particularly on the fluid Lorentz factor γ_d, momentum p_d, and electric field E_{zd} at the end of the driver. The dependence of the wake amplitude γ_m on fluid quantities in the wake will be determined in the subsequent section.

Under the assumption that $d\log(n)/dz \ll k_p(z)$ for all z, i.e. the plasma density gradients are long compared to the wake period scale, to lowest order the wake may be assumed to follow the uniform plasma solution with local density $n(z)$. Hence, the density in the wake $n_w(\zeta; z)$ is a function of ζ and is parameterized by z, i.e. by the local density $n(z)$.

Because $n(z)$ changes slowly compared to $n_w(\zeta, z)$, we find the dependence of $n_w(\zeta, z)$ at fixed z. In this section we will stop explicitly writing the z dependence, i.e. $n_w(\zeta; z) = n_w(\zeta)$ and $n = n(z)$.

The AP solution to the cold relativistic fluid equations has the form [36, 38]

$$\omega_p\zeta = \frac{2}{\kappa'}E(\varphi,\kappa^2) - \kappa' F(\varphi,\kappa^2) - \frac{1}{\beta}\frac{2\kappa}{\kappa'}\sin\varphi \,, \tag{8a}$$

$$\gamma(\varphi) = \gamma_m - (\gamma_m - 1)\sin^2(\varphi) \,, \tag{8b}$$

$$p(\varphi,\gamma) = \cos\varphi\sqrt{\gamma_m - 1}\sqrt{1+\gamma} \,, \tag{8c}$$

$$qE_z(\varphi) = \sin\varphi\sqrt{2(\gamma_m - 1)} \,, \tag{8d}$$

$$\beta(\varphi,\gamma) = p(\varphi,\gamma)/\gamma \,, \tag{8e}$$

$$n_w(\beta) = n\cdot(1-\beta)^{-1} \,, \tag{8f}$$

$$\kappa^2 = \frac{\gamma_m - 1}{\gamma_m + 1} \,, \tag{8g}$$

$$\kappa'^2 = \frac{2}{\gamma_m + 1} \,, \tag{8h}$$

where $F(\varphi,\kappa^2)$ and $E(\varphi,\kappa^2)$ are elliptic integrals of the first and second kind, respectively, and parameters $\varphi = 2n\pi$ correspond to maxima in the plasma density and $\varphi = j + \pi/2$, where $j \in \mathbb{Z}$, correspond to points of zero perturbation, $n_w = n$. Furthermore, we will demonstrate soon that $\varphi = (2j + 3/2)\pi$ corresponds to points of zero perturbation and increasing plasma density, $\partial n_w/\partial\zeta > 0$. These equations completely describe the wake behind the

drive electron beam given the mapping from drive beam to amplitude γ_m and starting parameter φ_{st}.

With the wake behind the driver completely described in terms of amplitude γ_m and parameter φ_{st}, the quantities ζ_δ and $\left.\frac{\partial(\omega_p^2/\gamma)}{\partial\zeta}\right|_{\zeta_\delta}$ may be derived. The position ζ_δ, measured from the leading edge of the drive beam, can be expressed as

$$\zeta_\delta = \zeta(3\pi/2) - \zeta(\varphi_{st}) + L_d/c \,, \tag{9}$$

where $\zeta(\varphi)$ is the position in the undriven wake as a function of φ, L_d is the length of the drive beam, and φ_{st} is determined so that the wake is continuous across the transition from drive beam to undriven wake. To enforce continuity of the wake, we will require that electric field and momentum are continuous at the transition from within the drive beam to behind the drive beam. Let γ_d denote the plasma Lorentz factor at the end of the drive beam, p_d be the plasma momentum at the end of the drive beam, and E_{zd} the electric field at the end of the driver. The equations for p and E_z behind the driver can be arranged to determine φ in terms of fluid quantities:

$$\cos\varphi = \frac{p}{\sqrt{\gamma_m - 1}\sqrt{1+\gamma}} \tag{10a}$$

$$\sin\varphi = \frac{qE_z}{\sqrt{2(\gamma_m - 1)}} \tag{10b}$$

These equations combine to determine $\tan\varphi_{st}$ as a function of the fluid quantities:

$$\tan\varphi_{st} = \frac{qE_{zd}}{p_d}\sqrt{\frac{1+\gamma_d}{2}} \,. \tag{11}$$

Now φ_{st} is determined by the fluid quantities within the drive beam. The dependence of these on the drive beam parameters will be derived in the next section.

Next the dependence of $\left.\frac{\partial(\omega_p^2/\gamma)}{\partial\zeta}\right|_{\zeta_\delta}$ on the unperturbed plasma density n and the wake amplitude γ_m is determined. Because ω_p^2 is proportional to n_w with constant of proportionality $e^2/m_e\varepsilon_0$, it suffices to calculate $\partial(n_w/\gamma)/\partial\zeta|_{\zeta_\delta}$. Because evolution in z is considered to be much slower than evolution in ζ, in this section n, ω_p, $\gamma_m(z)$, β, κ, and κ' are treated as constants. Hence all quantities ultimately depend only on ζ and we will derive $d(n_w/\gamma)/d\zeta|_{\zeta_\delta}$. When $\delta n = 0$, then $n_w = n$ so $\beta = p = 0$, $\gamma = 1$, and $\varphi = \varphi_j \equiv (j + 1/2)\pi$ with $j \in \mathbb{Z}$.

First, we note that $\left.\frac{d(n_w/\gamma)}{d\zeta}\right|_{\zeta_\delta} = \left.\frac{dn_w}{d\zeta}\right|_{\zeta_\delta}$, by observing that $\left.\frac{d\gamma}{d\zeta}\right|_{\zeta_\delta} = 0$. Then, because $\gamma_m(\varphi_j) = 1$, we have

$$\left.\frac{d(n_w/\gamma)}{d\zeta}\right|_{\zeta_\delta} = \left.\frac{dn_w}{d\zeta}\right|_{\zeta_\delta} = \left.\frac{dn_w}{d\beta}\right|_{\beta=0}\left.\frac{d\beta}{d\varphi}\right|_{\varphi=\varphi_j}\left.\frac{d\varphi}{d\zeta}\right|_{\zeta_\delta} . \tag{12}$$

Performing the substitutions yields the plasma gradient where $\delta n = 0$:

$$\left.\frac{dn_w}{d\zeta}\right|_{\zeta_\delta} = n(z)\left(-\sin(\varphi_j)\right)\sqrt{2(\gamma_m - 1)}\omega_p(z) \,. \tag{13}$$

The positive plasma gradient required for positive frequency shift then means we want odd values of j, i.e. for $l \in \mathbb{Z}$, values $\varphi_{2l+1} = (2l + \frac{3}{2})\pi$. We can now write

$$\left.\frac{d(\omega_p^2/\gamma)}{d\zeta}\right|_{\zeta_\delta} = \omega_p(z)n(z)\sqrt{2(\gamma_m - 1)} \,. \tag{14}$$

In this section, we have modeled the wake behind the driver as a traveling relativistic plasma wave. We presented a periodic parameterization of this wave and derived from this representation quantities ζ_δ and $\left.\frac{\partial\omega_p^2/\gamma}{\partial\zeta}\right|_{\zeta_\delta}$ necessary for understanding frequency shift and phase matching. It remains to determine the dependence of the amplitude γ_m on the drive beam density n_d and length L_d, as well as the dependence of fluid quantities at the end of the drive beam on the drive beam parameters. The quantities we want at the drive beam end are the electric field E_{zd}, fluid momentum p_d, and fluid gamma factor γ_d.

A. Solution within drive beam

In the previous section we determined the dependence of ζ_δ and $\left.\frac{\partial(\omega_p^2/\gamma)}{\partial\zeta}\right|_{\zeta_\delta}$ on the values of the fluid electric field, momentum, and Lorentz factor at the end of the drive beam, E_{zd}, p_d, and γ_d. To determine these expressions, we determine the fluid equations within the drive beam as a function of ζ and evaluate the solution at the end of the drive beam, $\zeta = L_d$. We follow the solution technique in Ref. [32], parameterizing the fluid quantities by a quantity x:

$$\gamma = \frac{1+x^2}{2x} \,, \tag{15a}$$

$$p = \frac{1-x^2}{2x} \,, \tag{15b}$$

$$E_z = \frac{\partial x}{\partial\zeta} = \mathrm{sgn}(E_z)\sqrt{2\left(1 - \frac{n_d}{n}\right) - \frac{1}{x} + \left(\frac{2n_d}{n} - 1\right)x} \,, \tag{15c}$$

$$\phi = 1 - x \,. \tag{15d}$$

The parameter x satisfies the equation

$$\frac{\partial^2 x}{\partial\zeta^2} = \frac{1}{2}\left(\frac{1}{x^2} - 1 + \frac{2n_d}{n}\right) \,. \tag{16}$$

The form of the solution is different for each of the three cases $0 < n_d < n/2$, $n_d = n/2$, and $n_d > n/2$; see Appendix A for the full derivation. We write here the expressions for the parameter x at $\zeta = L_d$, denoted x_d, in the three cases.

1. *Low density drive beam:* $0 < n_d < n/2$

This is the case studied in Rosenzweig [32]. Here x_d is a function of an intermediate variable θ_d which is determined implicitly as a function of L_d:

$$(1 - 2n_d/n)k_p L_d = 2\left[E(\sqrt{2n_d/n}) - E(\theta_d, \sqrt{2n_d/n})\right] , \tag{17a}$$

$$x_d = 1 + \frac{2n_d/n}{1 - 2n_d/n}\cos^2\theta_d , \tag{17b}$$

$$\mathrm{sgn}(E_{zd}) = \mathrm{sgn}\sin(2\theta_d) . \tag{17c}$$

2. *Drive beam density equal to background density:* $n_d = n/2$

The quantity x_d is determined implicitly from the equation

$$k_p L_d = \sinh^{-1}\sqrt{x_d - 1} + \sqrt{x_d - 1}\sqrt{x_d} ; \tag{18}$$

also, $\mathrm{sgn}(E_{zd}) = +1$.

3. *High density drive beam:* $n_d > n/2$

x_d is a function of θ_d, which is implicitly a function of n_d and L_d, and $E_{zd} > 0$:

$$(2n_d/n - 1)k_p L_d = 2\sqrt{2n_d/n} \times \ldots$$
$$\left(k'^2 F(\theta_d, k) - E(\theta_d, k) + \tan\theta_d\sqrt{1 - k^2\sin^2\theta_d}\right) , \tag{19a}$$

$$x_d = 1 + \tan^2\theta_d , \tag{19b}$$

$$\mathrm{sgn}\, E_{zd} = +1 . \tag{19c}$$

B. Discussion of wake solutions within driver

In each of the cases $n_d > n/2$, $n_d = n/2$, and $n_d < n/2$, we can use Eqns. (15) to determine the fluid Lorentz factor γ, the plasma electric field E_z, and the fluid momentum p as functions of x within the driver. The dependence of x on ζ is implicit. In each case, we found the dependence of x_d and the sign of E_{zd} on n_d and L_d.

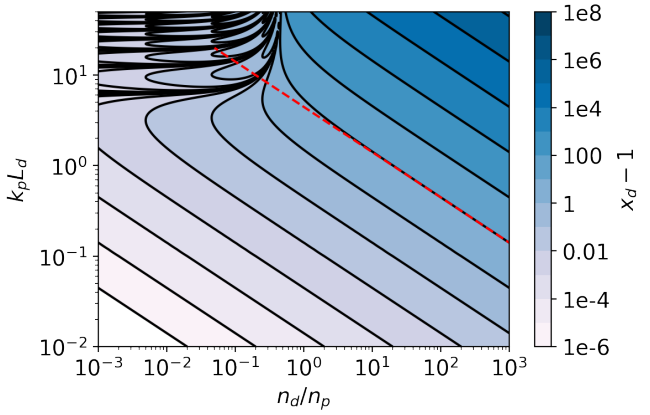

FIG. 1: Dependence of the parameter x_d on the drive beam parameters $k_p L_d$ and n_d/n. The dashed red line indicates the trajectory a dePWPA solution starting at $(k_p L_d, n_d/n) = (20, 0.0375)$ takes in $(k_p L_d, n_d/n)$. The solution is parameterized by the plasma density $n : 1 \to 0$. Note the constancy of x_d with n as $k_p L_d$ gets small or n_d/n gets large; this is a prediction of the short or high-density (SHD) approximation discussed in section V.

In Fig. 1 the dependence of x_d on drive beam parameters is presented. With γ_d, p_d, and E_{zd}, we can evaluate the continuity condition for φ_{st} using equation (11) as determined in Section III.

As discussed by Rosenzweig [32], we know from the continuity of the wake that

$$\gamma_m = \frac{1}{2}\left(\left.\frac{\partial x}{\partial\zeta}\right|_{L_d}\right)^2 + \gamma_d = 1 - \frac{n_d}{n} + \frac{n_d x_d}{n} . \tag{20}$$

If we recall that $\varphi_d = 1 - x_d$, we can express the wake amplitude in terms of fluid quantities just as we did $\varphi_s t$. Just as with the other fluid quantities γ_d, p_d, and E_{zd}, we know the potential ϕ_d in terms of x_d and x_d implicitly in terms of drive beam parameters n_d, L_d. Hence the equation for γ_m,

$$\gamma_m = 1 - \phi_d n_d/n , \tag{21}$$

is the final equation needed to describe ζ_d and $\left.\frac{\partial\delta n}{\partial\zeta_\delta}\right|_{\zeta_\delta}$ in terms of the drive beam parameters.

Using the solutions in this section, we can determine the fluid quantities at the end of the drive beam γ_d, p_d, E_{zd}, and ϕ_d from the drive beam parameters n_d, L_d and the plasma density $n(z)$. We can then calculate φ_{st} and γ_m from the fluid quantities at the end of the drive beam. This map can be used to calculate the wake for any flat-top drive beam and any density n.

IV. OBTAINING PHASE MATCHED DENSITY PROFILE AND FREQUENCY

We found previously that we could determine a plasma density profile that would guarantee phase matching of a laser pulse and the position of positive density gradient in the wake of an electron beam if we could solve the system of equations (4) and (7):

$$\frac{d\omega^2}{dz} \simeq n^{3/2}\sqrt{2\left[\gamma_m - 1\right]}\,. \tag{22}$$

$$\frac{dn}{dz} \simeq \frac{1}{2}\frac{n}{\omega^2}\left[\frac{d\zeta_\delta}{dn}\right]^{-1}\,. \tag{23}$$

Using the work in the previous sections, we have maps from the drive beam parameters n_d, L_d and the unperturbed plasma density n to the ζ_δ, the position of positive density gradient where $\delta n = 0$, and $\gamma_m(n; n_d, L_d)$, the amplitude of the wake behind the drive beam. The function $\zeta_\delta(n; n_d, L_d)$ can be evaluated and differentiated numerically, yielding values for the gradient $d\zeta_\delta/dn$. Thus, we can close the system of equations (22)-(23) and numerically integrate the ordinary differential equations to obtain n, ω. We summarize the procedure for obtaining the density profile and frequency shift in algorithm 1, together with references to the relevant equations in the text. In figure 2 we show a sample profile as predicted by algorithm 1. This computation was performed for a drive beam with density $n_d = 0.4$, and length $L_d = 1$. The tapered density profile is shown on the left in (a) and the relative gain in frequency, ω/ω_0, is show on the right in (b). A numerical implementation of the algorithm is shared in Appendix B.

Algorithm 1 Determining the dePWPA wake profile

1: Input: Drive parameters n_d, L_d
2: Determine x_d implicitly from n_d, L_d ▷ Equations (A14), (A16), (A28)
3: Evaluate γ_d, p_d, E_{zd}, and ϕ_d as functions of x_d ▷ Equations (15)
4: Evaluate φ_{st} and γ_m as functions of γ_d, p_d, E_{zd}, and ϕ_d ▷ Equations (11), (21)
5: Use $\zeta_d(n)$ to numerically evaluate $\frac{\partial\zeta_d}{\partial n}$ ▷ Equation (9)
6: Numerically solve $\frac{d\omega^2}{dz} \simeq n^{3/2}\sqrt{2\left[\gamma_m - 1\right]}$, $\frac{dn}{dz} \simeq \frac{1}{2}\frac{n}{\omega^2}\left[\frac{d\zeta_\delta}{dn}\right]^{-1}$ ▷ Equations (22)(23)

Eqns. (22) and (23) are a coupled system of differential equations that can be evaluated to determine the density profile and expected frequency shift for phase matched photon acceleration driven by an ultrarelativistic beam driver. However, finding the variation of ζ_δ with density in the nonlinear case is a challenge as it is the solution of an implicit equation. This can be evaluated numerically for specific cases but is not tractable for analytic predictions of long-term behavior or scaling laws. Insight can be gained by using short or high-density driver approximations, for which an analytic solution can be found. This is presented in the following section.

V. SHORT AND HIGH-DENSITY DRIVER LIMITS, UNLIMITED PHOTON ACCELERATION, AND WEAK DRIVER LIMIT

In this section we consider phase matched photon acceleration in various limits to explain the pattern seen in Fig. 1, where the parameter x_d is constant with respect to n for small k_pL_d or large n_d/n. We investigate the plasma response behind the drive beam in both the short and high-density drive beam limits. In each case, we find $x_d \simeq 1 + \frac{n_d L_d^2}{2}$, as indicated in Fig. 1.

A. Short drive beam limit

First we consider the case $k_pL_d \ll 1$. Due to the qualitative distinction between drive beams of density $n_d/n > 1/2$ and $n_d/n < 1/2$, we consider the short drive beam limit in each case separately.

1. *Low density drive beam: $n_d < n/2$*

Recall the equations describing the plasma response behind a low-density beam, $n_d = n_d/n < 1/2$, are

$$(1 - 2n_d/n)k_pL_d = 2\left[E(\sqrt{2n_d/n}) - E(\theta_d, \sqrt{2n_d})\right], \tag{24a}$$

$$x_d = 1 + \frac{2n_d/n}{1 - 2n_d/n}\cos^2\theta_d\,, \tag{24b}$$

where $E(\theta, k) \equiv \int_0^\theta \sqrt{1 - k^2\sin^2\theta'}d\theta'$ and $E(k) \equiv E(\pi/2, k)$. In the limit $k_pL_d \ll 1$, Eqn. (24a) becomes

$$E(\sqrt{2n_d/n}) = E(\theta_d, \sqrt{2n_d/n}), \tag{25}$$

meaning $\theta_d \approx \pi/2$.

If we then expand around $\theta_d = \pi/2$ and approximate the integral in Eqn. (24a), we find

$$\begin{aligned} E(\sqrt{2n_d/n}) - E(\theta_d, \sqrt{2n_d/n}) \\ \simeq \sqrt{1 - 2n_d/n}(\pi/2 - \theta_d), \end{aligned} \tag{26}$$

and hence $\theta_d \simeq \pi/2 - \sqrt{1 - 2n_d/n}\,k_pL_d/2$. Then $\cos^2\theta_d \simeq \frac{1}{4}(1 - 2n_d/n)(k_pL_d)^2$. In these normalized units, $k_p = \sqrt{n}$ and thus

$$x_d \simeq 1 + \frac{n_d L_d^2}{2}. \tag{27}$$

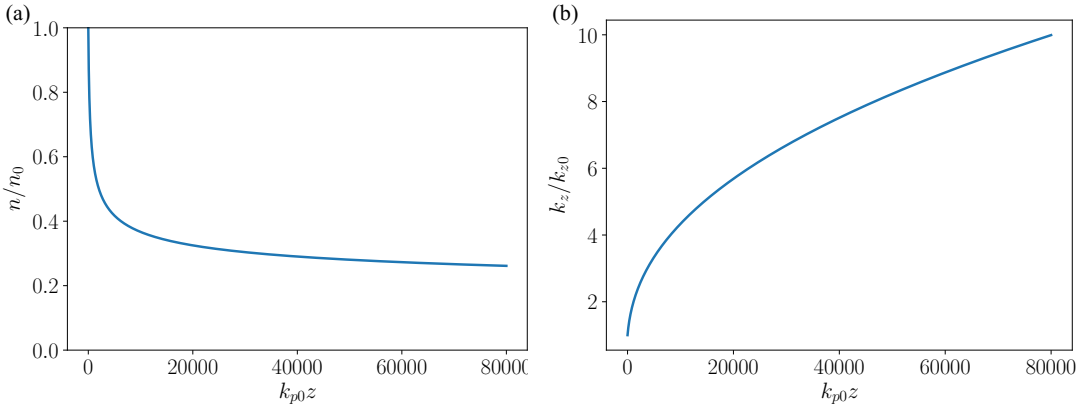

FIG. 2: Numerically determined profiles for unlimited photon acceleration, computed by algorithm 1 with $n_d = 0.4$, $L_d = 1$, and $A = 0.4$. (a) shows the computed plasma density and (b) shows the relative gain in laser frequency.

2. *High density drive beam: $n_d/n > 1/2$*

In this section we derive the plasma density response behind a high density, meaning $n_d/n > 1/2$, short ($k_p L_d < 1$) beam. The governing equations are:

$$x_d = 1 + \tan^2\theta_d, \tag{28a}$$

$$(2n_d/n - 1)k_p L_d = 2\sqrt{2n_d/n}\left(k'^2 F(\theta_d, k) - E(\theta_d, k) + \tan\theta_d\sqrt{1 - k^2\sin^2\theta_d}\right), \tag{28b}$$

$$k^2 = n/2n_d,\ k'^2 + k^2 = 1. \tag{28c}$$

It can be shown that the angle θ_d tends to 0 as $k_p L_d \to 0$. If we expand in small θ_d and approximate the integrals for F and E, we get

$$\begin{aligned}\left(\frac{2n_d}{n} - 1\right)k_p L_d = 2\sqrt{\frac{2n_d}{n}}\Bigg[&(1-k^2)\left(\theta_d + \frac{k^2\theta_d^3}{4} - \mathcal{O}(\theta_d^5)\right) - \left(\theta_d - \frac{k^2\theta_d^3}{4} + \mathcal{O}(\theta_d^5)\right)\ldots \\ &+ \left(\theta_d + \frac{\theta_d^3}{3} + \mathcal{O}(\theta_d^5)\right)\left(1 - \frac{k^2\theta_d^2}{2} + \mathcal{O}(\theta_d^4)\right)\Bigg]\end{aligned} \tag{29}$$

To lowest order in θ_d, this is

$$\theta_d = k_p L_d\sqrt{\frac{n_d}{2n}}. \tag{30}$$

Inserting in the x_d equation, Eqn. (28a), and keeping the lowest order in θ_d, we have again

$$x_d \simeq 1 + \frac{n_d L_d^2}{2}. \tag{31}$$

B. High-density drive beam limit

In this section we derive the plasma density of a very high density ($n_d/n \gg 1/2$) beam. As in the preceding section describing the short driver limit when $n_d > n/2$, Sec. V A 2, the plasma response follows the $n_d > n/2$ equations, Eqns. (28).

If k is small than the integrand of the elliptic function $F(\theta_d, k)$ simplifies and F becomes:

$$F(\theta_d,k)=\int_0^{\theta_d}\frac{1}{\sqrt{1-k^2\sin^2\varphi}}d\varphi \tag{32}$$

$$\simeq\theta_d\left(1+\frac{k^2}{4}\right)-\frac{k^2}{8}\sin 2\theta_d\ . \tag{33}$$

Similarly,

$$E(\theta_d,k)=\theta_d\left(1-\frac{k^2}{4}\right)+\frac{k^2}{8}\sin 2\theta_d\ . \tag{34}$$

Then Eqn. (28b) becomes

$$\sqrt{\frac{n_d}{2n}}k_pL_d\simeq k'^2\left[\theta_d\left(1+\frac{k^2}{4}\right)-\frac{k^2}{8}\sin 2\theta_d\right]\left[\theta_d\left(1-\frac{k^2}{4}\right)+\frac{k^2}{8}\sin 2\theta_d\right]+\tan\theta_d\left(1-\frac{k^2}{2}\sin^2\theta_d\right). \tag{35}$$

To lowest order in k, $\tan\theta_d=\sqrt{\frac{n_d}{2}}L_d$ and

$$x_d\simeq 1+\frac{n_dL_d^2}{2}\ . \tag{36}$$

C. Implications of the short and high-density limits

As long as the drive beam is not both long and low density, the plasma response behind the driver is characterized by $x_d=1+\frac{n_dL_d^2}{2}$. Then the wake amplitude is $\gamma_m\simeq 1+\frac{n_d^2L_d^2}{2n}$.

The areal beam charge density $A\equiv n_dL_d$ is a measure of the strength of the drive beam, especially in the short drive beam limit. The wake amplitude is

$$\gamma_m=1+\frac{A^2}{2n}\ . \tag{37}$$

Hence, the frequency shift relation, Eqn. (22), in the short/high-density limit is

$$\frac{d\omega^2}{dz}=nA\ . \tag{38}$$

Eqns. (38) and (23) may be combined,

$$\frac{d\omega^2}{dz}=\frac{d\omega^2}{dn}\frac{dn}{dz}=2A\omega^2\frac{d\zeta_\delta}{dn}\ , \tag{39}$$

and directly integrated,

$$\int_{\omega_0}^{\omega}\frac{1}{\omega'^2}d\omega'=2A\int_{n_0}^{n}\frac{d\zeta_\delta}{dn'}dn'\ , \tag{40}$$

to obtain

$$\omega(n)=\omega_0\exp\left[A\left(\zeta_\delta(n)-\zeta_{\delta 0}\right)\right]\ , \tag{41}$$

defined for n in $(0,n_0]$ where $n(0)=n_0$.

The matched phase in the wake, ζ_δ, also has a simpler expression in the SHD approximation. Since the width of the beam vanishes, the wake starts at phase $\varphi_0=\pi/2$ and the expression for ζ_δ is:

$$\zeta_\delta=\zeta(3\pi/2)-\zeta(\pi/2)=\frac{1}{\omega_p}\left[\frac{4}{\kappa'}E(\kappa)-2\kappa'K(\kappa)+4\frac{\kappa}{\kappa'}\right]\ , \tag{42}$$

where $\kappa^2=(1+4n/A^2)^{-1}$ and $\kappa'^2=(1+A^2/4n)^{-1}$.

Larger frequency shifts require lower densities and longer propagation distances. For a given frequency ω to be realized, equation (41) indicates the what plasma density n must be attained. Then the propagation distance z can be determined as a function of n. The differential relation between z and n is

$$\frac{dz}{dn}=\frac{d\omega^2}{dn}\frac{dz}{d\omega^2}=\frac{2\omega^2}{n}\frac{d\zeta_\delta}{dn}\ . \tag{43}$$

This equation can be integrated to give

$$z=2\omega_0^2\int_{n_0}^{n}\frac{1}{n'}\frac{d\zeta_\delta}{dn'}e^{2A(\zeta_\delta(n)-\zeta_{\delta 0})}dn'\ . \tag{44}$$

Equations (41) and (44) provide a complementary and more analytic method of determining density profiles and frequency shifts to the numerical integration of equations (22) and (23).

D. Unlimited photon acceleration

Since $d\omega^2/dz>0$ and $dn/dz<0$, there are no fixed points or periodic orbits and so, by the Poincaré-Bendixon theorem, there are no limit sets to the orbits. In fact, we demonstrate that as $n\to 0$, $\zeta_\delta(n)\to\infty$ and $\omega(n)\to\infty$.

Recall that $\kappa^2=\frac{A^2}{4n+A^2}\to 1$ as $n\to 0$ and so $\kappa'^2\to 0$. It can be shown [40] that $E(\kappa)\to 1$ as $\kappa\to 1$ and

$$K(\kappa)\sim\ln\frac{4}{\kappa'}\qquad\text{as}\qquad\kappa\to 1\ . \tag{45}$$

Now ζ_δ simplifies to

$$\begin{aligned}\zeta_\delta&\sim\frac{1}{\sqrt{n}}\left[\frac{4}{\kappa'}(1+1)-2\kappa'\ln\frac{4}{\kappa'}\right]\\&\sim\frac{1}{\sqrt{n}}\frac{8}{\kappa'}\to\infty\qquad\text{as}\qquad n\to 0\ .\end{aligned} \tag{46}$$

From Eqn. (41), the laser frequency ω is unbounded as plasma density tends to 0. This 'unlimited photon acceleration' (see also Bulanov et al. [22] for some discussion

of unlimited particle acceleration) is quite significant in that a physical mechanism for frequency shift is now rigorously proven to admit arbitrary frequency shifts, provided that the drive beam can be sustained.

E. Weak driver limit

For a moderate strength driver, $A < 1$, the function $\zeta(n)$ is

$$\omega_p \zeta = \varphi - \frac{A}{n^{1/2}} \sin\varphi + \frac{A^2}{16n}(3\varphi + \sin 2\varphi) \,. \tag{47}$$

The location of the zero density perturbation, ζ_δ, can be described accurately by the expansion

$$\zeta_\delta = \frac{\pi}{n^{1/2}} + \frac{2A}{n} + \frac{3\pi}{16}\frac{A^2}{n^{3/2}} + \cdots \,. \tag{48}$$

Retaining up to the third term in this expansion, the phase-matching relation, Eqn. (23), is

$$\frac{dn}{dz} = -\frac{n^{5/2}}{\pi\omega^2}\left(1 + \frac{4\pi A}{n^{1/2}} + \frac{9A^2}{16n}\right)^{-1} \,. \tag{49}$$

The expansions developed in this section are seen to be accurate over a large parameter range. In figure 3 we present γ_m, ζ_d, n, and k_L for $A = 0.01, 0.1, 1$, and 10 and for $L_{d0} = 0.01$. This short driver length guarantees that the SHD limit holds very well. This is why the dashed and solid lines in the top row, which shows the wake amplitude γ_m, agree so well for all A. The second row shows the position of 0 density perturbation ζ_δ and its approximations, which agree with the exact function to $A = 1$. The next rows show the predicted density profile and frequency gain. The density profile is accurately predicted with the expansion for A as large as 1. The slow variation in n in all cases means that the predicted frequency gain of the analytic expansion matches the numerical prediction for all values of A calculated. We see that generally the expansion is good for $A = 1$ and surprisingly accurate even for $A = 10$.

VI. CONCLUSIONS

In conclusion, we have given the details for an analytic model for a plasma density profile that achieves phase matching for a beam driven plasma wakefield accelerator. The model predicts arbitrary frequency shift limited only by depletion of the drive beam. This model was used to generate the density profiles used in Ref. [31] that were used in ab-initio relativistic electromagnetic particle-in-cell simulations. The simulations in that paper were both one- and three-dimensional; the one-dimensional solutions were demonstrated to be effective in three dimensions in the broad-driver regime, as expected. The algorithm developed should enable other researchers to easily study the dePWPA scheme.

The mathematical 1D dePWPA model assumes an ultrarelativistic driver moving at the speed of light. Given these assumptions, the frequency shift is arbitrarily large ('unlimited'). In practice, these assumptions are violated and this imposes some limitations on the frequency shift that is realizable and hence we discuss some of these limitations here.

The treatment of the wake behind the drive beam as an AP wave assumes a cold 1D plasma and that $\gamma_m < \gamma_d$; if this condition is not met, the AP wave breaks. Background plasma particles can be trapped in the wake, the fields and density profile are altered, and in particular the plasma density gradient differs from the AP model. Wave breaking is not considered in this manuscript but would limit the achievable frequency shift. For the ultrarelativistic drive beam approximation assumed in our work, $v_d \to c$, the Lorentz factor $\gamma_d \to \infty$ and the AP condition is always met. Given a realistic driver with $v_d < c$, the AP wave breaks when $\gamma_m \geq \gamma_d$. Consider, for example, a 10 GeV electron beam driver for which $\gamma_d \approx 20000$, with normalized areal beam charge density $A \sim 1$. In this case, using the ultrashort beam limit described above for γ_m, the wavebreaking condition occurs when $20000 = 1 + A^2/2n$, so the limit can be estimated using $A^2/n \sim 10^4$, i.e. n would drop to 10^{-4} of its initial value. Hence, the plasma frequency would drop to 10^{-2} of its initial value and the relativistic plasma wavelength would increase by a factor $\mathcal{O}(100)$. Now recall the frequency shift scaling from Eqn. 41, $\omega(n) = \omega_0 \exp(A(\zeta_\delta(n) - \zeta_{\delta 0}))$. The position of the laser, ζ_δ, scales with the plasma wavelength. We can therefore estimate that wavebreaking occurs for these parameters when the laser frequency has increased by a factor of $\exp(\mathcal{O}(100))$; wave breaking is evidently not a very restrictive limit in the cold 1D model.

On the other hand, it is well known [41] that the wavebreaking threshold is lowered by finite plasma temperature. Including the effect of finite plasma temperature may more significantly limit the achievable frequency shift and would be an interesting direction of future work. More importantly for experimental realization of dePWPA, transverse motion and 3D effects were also not considered in this manuscript. Although we showed in our paper [31] that in practice the 1D solutions could be used reasonably in the 3D case, inclusion of transverse effects introduces additional wavebreaking mechanisms and qualitative changes to the wake profile that would affect the asymptotic limits presented here. For example, if the plasma is driven hard enough that the plasma electrons can be completely expelled from the wake, it may form a spherical cavity of positive charge behind the driver, known as the blowout [42] / bubble [43] regime. In the blowout regime, the smoothly varying plasma gradient becomes very steep in a narrow sheath region around the bubble. While this steep gradient may provide enhanced photon acceleration, the laser pulse is likely to be much longer than the scale length of the density gradient and may not be well modeled by the dePWPA

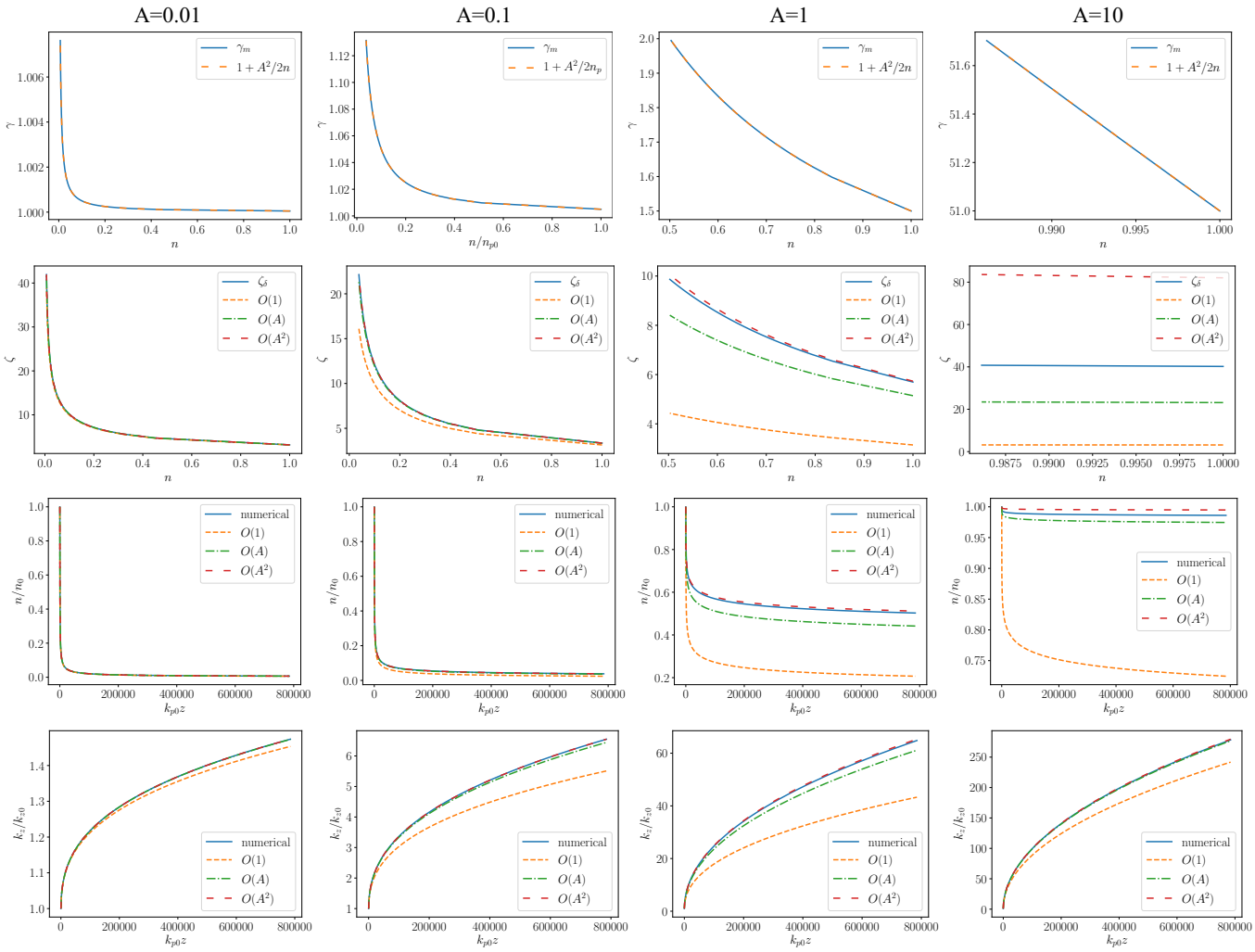

FIG. 3: Comparing numerical and short or high-density small A expansions. We show that the wake amplitude γ_m, the position of 0 density perturbation ζ_δ, and the predicted density n and frequency gain k_L/k_{L0} profiles for $A = 0.01, 0.1, 1$, and 10 when $k_{p0}L_{d0} = 0.01$. The length satisfies $k_{p0}L_d \ll 1$ so $\gamma_m = 1 + A^2/2n$ is always accurate. The expansion to $\mathcal{O}(A^2)$ is quite accurate for ζ_δ,n, and k_L for A as large as 1. The expansion when $A = 10$ is not good for ζ_δ but is surprisingly accurate in predicting n and k_L even for $A = 10$.

scheme presented in this paper. Moreover, the size of the wake and particularly the position ζ_δ are different in the blowout regime than in the 1D PA wave. Several 3D wakefield models for the bubble regime have been put forward in the literature that agree well with PIC simulation results [44–46]; it would be interesting to investigate whether the dePWPA theory can be extended to include the 3D nonlinear model of the blowout in calculating ζ_δ and $d\zeta_\delta/dn$ and whether photon acceleration can still be effective in the blowout regime.

Laser-driven dephasingless photon acceleration, a deLWPA scheme, would be of interest. The evolution of a laser pulse is very different from an electron beam so LWPA theoretically is a separate research topic. However, there are new spatiotemporal pulse-shaping techniques (that generate a so-called 'flying focus'), that would enable a laser pulse with group velocity that mimics the rigid motion of an ultrarelativistic electron beam driver [47, 48]. In this case we anticipate that minor modifications to the dePWPA theory would accommodate similar frequency shifts driven by a laser pulse with flying focus, similar to previous work using an ionization front [23].

ACKNOWLEDGMENTS

This work was supported by AFOSR grant FA9550-19-1-0072 and NSF grant 1804463. Computational resources were provided by Advanced Research Computing at the University of Michigan. The authors would like to acknowledge the OSIRIS Consortium, consisting of UCLA

and IST (Lisbon, Portugal) for providing access to the OSIRIS 4.0 framework.

Appendix A: Details of the solution for the wake within the driver

In this appendix we determine the map from drive beam parameters to wake behind the driver. In the previous section we found that the wake behind the driver can be completely understood in terms of its amplitude γ_m and a continuity condition between the wake within the drive beam and the wake behind the drive beam. The continuity condition depends on the plasma particle Lorentz factor γ_d, momentum p_d, and electric field E_{zd} at the end of the drive beam. In this section we derive γ_m, γ_d, p_d, and E_{zd} in terms of the drive beam parameters. To determine the wake quantities at the end of the drive beam, we solve the fluid equations with nonzero drive beam density.

This section consists of three parts. First, the plasma fluid equations within the drive beam are presented. Next, these are solved in three cases depending on the relation between the drive beam density n_d and the unperturbed plasma density $n = n(z)$, namely when $n_d > n/2$, $n_d = n/2$, and $n_d < n/2$. Since there are three solution sets, the quantities γ_d, p_d, and E_{zd} are expressed in three different cases. The electric potential at the end of the driver, ϕ_d, we also be presented in each case, since it is needed for determining the amplitude γ_m of the wake behind the driver. This section ends by deriving the relation $\gamma_m = 1 - n_d\phi_d$ between the drive beam parameters and the amplitude of the wake behind the driver.

We begin with the plasma fluid equations within the drive beam. We assume an ultrarelativistic ($\beta_d \to 1$) drive beam, in which case the fluid equations are

$$\frac{n_w}{n} = \frac{1}{1-\beta} \,, \tag{A1a}$$

$$\frac{1}{\omega_p^2}\frac{\partial^2}{\partial\zeta^2}(\gamma(1-\beta)) = \frac{\beta}{1-\beta} + \frac{n_d}{n} \,. \tag{A1b}$$

Using the approximation that the plasma density $n(z)$ is slowly varying, we may use the wake solutions in constant density to find $n_w(\zeta; n(z))$. We therefore treat $n(z)$ as a constant, n, and write $\zeta = \omega_p\zeta$, $n_d = n_d/n$, and $L_d = \omega_p L_d/c$. This normalization was not used in the text to prevent confusion when incorporating the variation of $n(z)$. Here, however, in the context of determining the wake profile, the constant density assumption permits the convenient suppression of n.

Following Rosenzweig [32], we let

$$x(\zeta) \equiv \gamma(1-\beta) = \sqrt{\frac{1-\beta}{1+\beta}} \,. \tag{A2}$$

This leads to

$$\frac{\partial^2 x}{\partial\zeta^2} = \frac{1}{2}\left(\frac{1}{x^2} - 1 + 2n_d\right) \,. \tag{A3}$$

We assume that the plasma is quiescent ahead of the driver, so for $\zeta \le 0$, $\beta = 0 = p = E$, and $n = 1 = \gamma = x$.

This integrates once to give

$$\left(\frac{\partial x}{\partial\zeta}\right)^2 = 2(1-n_d) - 1/x + (2n_d - 1)x \,. \tag{A4}$$

We make a detour to discuss the electric field and the choice of sign for the square root that equals $\frac{\partial x}{\partial\zeta}$. Recall that Gauss' law in this ultrarelativistic problem states

$$\begin{aligned} -\frac{1}{v_d}\frac{\partial E_z}{\partial\zeta} &= 4\pi e(n_i - n_e - n_d) \,, \\ \frac{\partial E_z}{\partial\zeta} &= -(1 - n_w - n_d) = \frac{\partial^2 x}{\partial\zeta^2} \,. \end{aligned} \tag{A5}$$

We can make the identifications $E_z = \pm\frac{\partial x}{\partial\zeta}$ and $\phi = \pm(-x+1)$ since $E_z = 0 = \frac{\partial x}{\partial\zeta}$ for $\zeta \le 0$. Since we made the assumption that the plasma species and beam particles are electrons, immediately behind the driver the electron density is decreased; then $\frac{\partial E_z}{\partial\zeta} = n_w + n_d - 1 > 0$ and we start with the positive square root for $\frac{\partial x}{\partial\zeta}$.

For identifying dependence of fluid quantities on drive beam parameters we identify dependence on x:

$$\gamma = \frac{1+x^2}{2x} \,, \tag{A6a}$$

$$p = \frac{1-x^2}{2x} \,, \tag{A6b}$$

$$E_z = \frac{\partial x}{\partial\zeta} = \mathrm{sgn}(E_z)\sqrt{2(1-n_d) - 1/x + (2n_d-1)x} \,, \tag{A6c}$$

$$\phi = 1 - x \,. \tag{A6d}$$

The sign of E_z can change in some cases; we comment in each case whether E_z stays positive or not and how to determine the sign of E_{zd}.

In Eqn. (A4), the term $(2n_d - 1)x$ changes sign based on the relation of n_d and $1/2$, as does the qualitative behavior of the solution and the technique used to derive the solution. There are three cases to consider:

1. $\mathbf{0 < n_d < 1/2}$

This is the case studied in Rosenzweig [32]; the equation for x is

$$\frac{\partial x}{\partial\zeta} = \sqrt{2 - 2n_d - 1/x - (1-2n_d)x} \,. \tag{A7}$$

Following Rosenzweig, we perform a change of variables to

$$(x-1)(1-2n_d) \equiv 2n_d \cos^2\theta \ , \tag{A8}$$

and write the solution as an implicit relation for θ as a function of ζ:

$$(1-2n_d)\zeta(\theta) = 2(E(\sqrt{2n_d}) - E(\sqrt{2n_d},\theta)) \ , \tag{A9}$$

where

$$E(\theta,k) \equiv \int_0^\theta \sqrt{1-k^2\sin^2\theta'}d\theta' \tag{A10}$$

is the incomplete elliptic integral of the second kind and $E(k) = E(\pi/2,k)$ is the corresponding complete integral of the second kind.

The above relation is valid within the driver, for $-L_d \leq \zeta \leq 0$. Solving for $\theta(\zeta)$, we can find x:

$$x(\zeta) = 1 + \frac{2n_d}{1-2n_d}\cos^2\theta(\zeta) \ . \tag{A11}$$

Here $x(\zeta)$ is oscillatory, so determining the electric field requires determining sign changes. Since the electric field is equal to $\pm\frac{\partial x}{\partial \zeta}$, $\frac{\partial x}{\partial \theta} = \frac{2n_d}{1-2n_d}\sin 2\theta(\zeta)$, and

$$\frac{\partial\theta}{\partial\zeta} = \frac{2n_d-1}{2\sqrt{1-n_d\sin^2\theta}} > 0 \ , \tag{A12}$$

we know that

$$\mathrm{sgn}(E_z) = \mathrm{sgn}\sin 2\theta \ . \tag{A13}$$

In summary, x_d is a function of an intermediate variable θ_d which is determined implicitly from the following equations:

$$(1-2n_d)L_d = 2\left(E(\sqrt{2n_d}) - E(\theta_d,\sqrt{2n_d})\right) \ , \tag{A14a}$$

$$x_d = 1 + \frac{2n_d}{1-2n_d}\cos^2\theta_d \ , \tag{A14b}$$

$$\mathrm{sgn}(E_{zd}) = \mathrm{sgn}\sin(2\theta_d) \ . \tag{A14c}$$

2. $\mathbf{n_d = 1/2}$

In this case the equation for x simplifies to

$$\frac{\partial x}{\partial\zeta} = \sqrt{1-\frac{1}{x}} \ . \tag{A15}$$

Since $\frac{\partial\zeta}{\partial x} > 0$ at $x = 1$, $\zeta = 0$, $\frac{\partial x}{\partial\zeta} > 0$ for all ζ and so $x(\zeta)$ is a positive, monotonically increasing function. In addition, as $x(\zeta)$ is non-oscillatory, E_z and n_w will be monotone and in particular E_z stays positive within the drive beam. Similarly the electric potential $\phi < 0$ within the drive beam.

The quantity x_d is determined implicitly from the equation

$$L_d = \sinh^{-1}\sqrt{x_d-1} + \sqrt{x_d-1}\sqrt{x_d} \tag{A16}$$

and $\mathrm{sgn}(E_{zd}) = +1$.

3. $\mathbf{n_d > 1/2}$

The equation for x is:

$$\frac{\partial x}{\partial\zeta} = \sqrt{2(1-n_d) - 1/x + (2n_d-1)x} \ . \tag{A17}$$

Note that this will stay positive, so x is a positive, monotonically increasing function of ζ. Rearranging so we can solve for $\zeta(x)$,

$$\frac{\partial\zeta}{\partial x} = \frac{\sqrt{x}}{\sqrt{x-(2n_b-1)x-1+(2n_b-1)x^2}} \ , \tag{A18}$$

and integrating, we have

$$\sqrt{2n_d-1}\int_0^\zeta d\zeta' = \int_1^x \frac{\sqrt{x'}}{\sqrt{(x'-1)\left(x'+\frac{1}{2n_d-1}\right)}}dx' \ . \tag{A19}$$

Following a similar vein to the solution technique for $n_d < 1/2$, we use the substitution:

$$(x-1)(2n_d-1) = t^2 \ , \tag{A20}$$

and arrive at

$$\sqrt{2n_d-1}\zeta = \frac{2}{\sqrt{2n_d-1}}\int_0^t \frac{\sqrt{t^2+2n_d-1}}{\sqrt{t^2+2n_d}}dt \ . \tag{A21}$$

The integral in Eqn. (A21) is an elliptic integral. We find a recipe for its evaluation in Eqns. (221.04) and (313.02) of Byrd and Friedman [40] :

$$\int_0^t \frac{\sqrt{t'^2+b^2}}{\sqrt{t'^2+a^2}}dt' = gb^2\left(\frac{1}{k'^2}\left\{k'^2F(\tan^{-1}\frac{t}{b},k) - E(\tan^{-1}\frac{t}{b},k) + \frac{t}{b}\sqrt{1-k^2\sin^2\left(\tan^{-1}\frac{t}{b}\right)}\right\}\right) , \tag{A22}$$

$$a^2 = 2n_d, \quad b^2 = 2n_d - 1, \quad g = \frac{1}{a} = \frac{1}{\sqrt{2n_d}}, \quad k^2 = \frac{a^2-b^2}{a^2} = \frac{1}{2n_d}, \quad k'^2 = 1-k^2 = \frac{2n_d-1}{2n_d} . \tag{A23}$$

Now we employ a trigonometric substitution,

$$\tan\theta = \frac{t}{b} , \tag{A24}$$

and, observing that

$$\frac{gb^2}{k'^2} = \frac{2n_d-1}{\sqrt{2n_d}}\frac{2n_d}{2n_d-1} \tag{A25}$$

$$= \sqrt{2n_d} , \tag{A26}$$

we arrive at

$$(2n_d-1)\zeta = 2\sqrt{2n_d}\times\ldots \\ \left(\ k'^2F(\theta,k) - E(\theta,k) + \tan\theta\sqrt{1-k^2\sin^2\theta}\right) . \tag{A27}$$

To complete the $n_d > n/2$ equations, we combine the substitutions in Eqns. (A20) and (A24) to get the equation for x_d as a function of θ_d and include the condition on sgn E_{zd}:

$$x_d = 1 + \tan^2\theta_d \tag{A28a}$$

$$\text{sgn } E_{zd} = +1 \tag{A28b}$$

To evaluate the accuracy of this map in each of the three cases, we compare the theoretical wake profile with the wake profile computed in 1D PIC simulations for drive beams of various lengths and of densities at, greater than, and less than the plasma densities. As seen in figure 4, the theoretical prediction agrees very well with the computed wake.

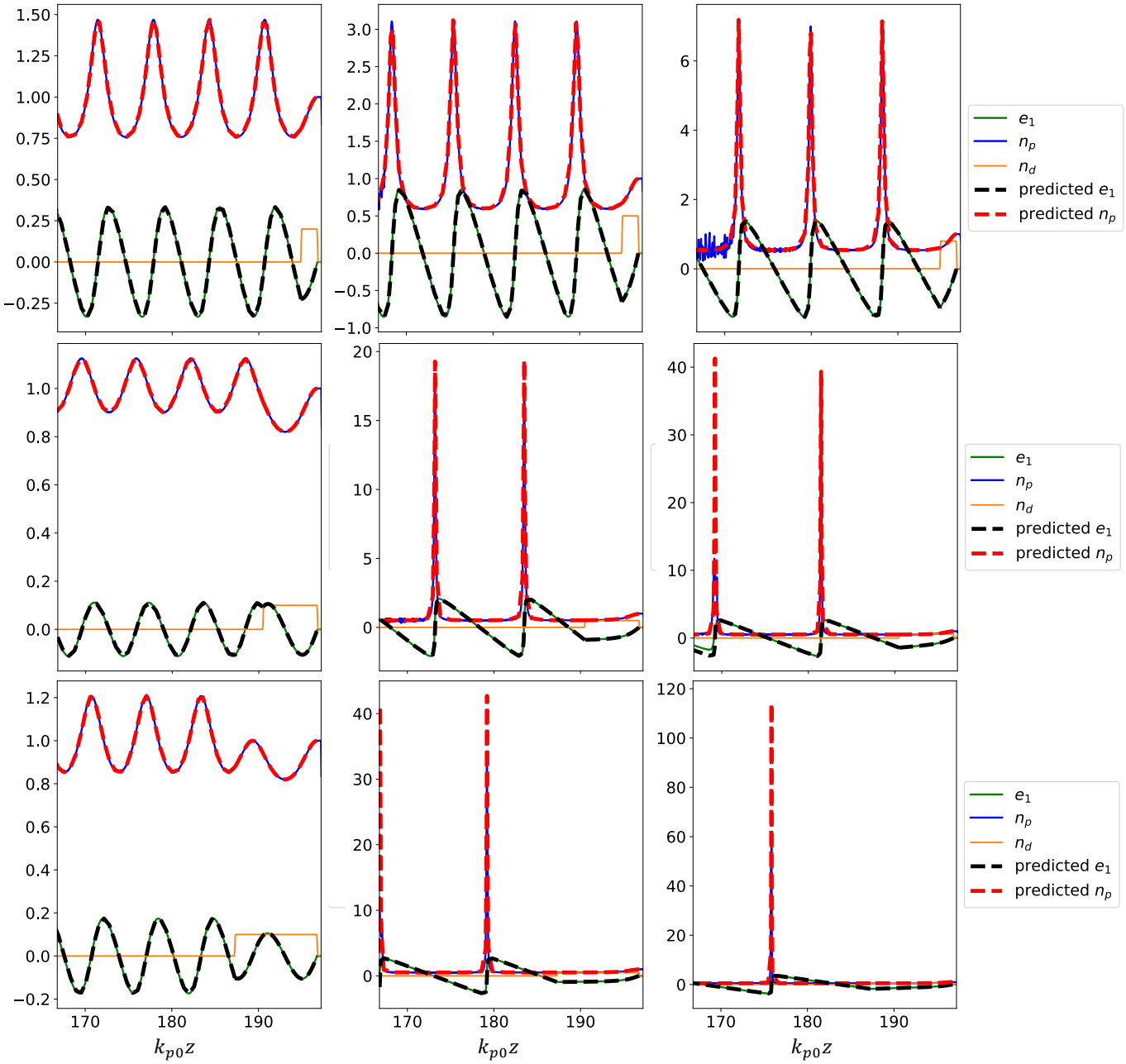

FIG. 4: Analytic expressions in the wake compared to OSIRIS 1D simulation data. Top row: $k_{p0}L_{d0} = 1.9, n_{d0}/n = 0.2, 0.5, 0.8$. Middle row: $k_{p0}L_{d0} = 6.28, n_{d0}/n = 0.1, 0.5, 0.6$ Bottom row: $k_{p0}L_{d0} = 9.5, n_{d0}/n = 0.1, 0.5, 0.6$. The expressions are exact in a uniform density plasma (here $n = 1$ but any value of n is possible).

Appendix B: Example code to obtain plasma density profile

In this section we present the practical evaluation of the dephasingless PWPA plasma density profile using a Python script. A sample Jupyter notebook is shown in figure 5 demonstrating usage of the code, along with a visualization of the resulting plasma density profile and laser frequency. To use this code to generate a plasma density profile in the Python-based PIC code FBPIC, we created an interpolating function based on the arrays returned by the Python dePWPA code. To generate a profile for the OSIRIS PIC code, the plasma density profile must be expressed in terms of elementary functions that are recognized by the OSIRIS function parser. We found that a function of the form $f(x) = a + b/(c + x)^d$ yielded a good fit for the plasma density profile.

The Python code itself, `dephasingless_pwpa_plasma_profile`, is provided in the supplementary material. The primary function in `dephasingless_pwpa_plasma_profile` is `get_depa_profile`, which takes as required input the initial critical-to-plasma-density ratio, the initial drive beam density, and the initial drive beam length and returns arrays of propagation distances, the plasma density profile at those distances, and the theoretical resulting frequency shift. This code is documented for ease of use, as shown in Fig. 6.

[1]:
```
import numpy as np
import matplotlib as mpl
from matplotlib import pyplot as plt
import dephasingless_pwpa_plasma_profile as depa
```

[2]:
```
nc0_np0 = 100
nd0_np0 = 0.2
kp0Ld0 = 1.9
lambda_L0 = 8e-7
lambda_p0 = lambda_L0 * np.sqrt(nc0_np0)
kp0 = 2*np.pi / lambda_p0
kp0z, n_n0_depa, k_kp0_depa = depa.get_depa_profile(nc0_np0,
                                                    nd0_np0,
                                                    kp0Ld0,
                                                    kp0z_final=80000,
                                                    n_steps=160001)
```

[4]:
```
mpl.rcParams.update({'font.size': 18})
```

[5]:
```
fig, axT = plt.subplots(1,2,figsize=(10,4.5))
ax = axT[0]
ax.plot(kp0z, n_n0_depa)
ax.set_xlabel(r'$\omega_{p0}t=k_{p0}z$')
ax.set_ylabel(r'$n/n_0$')
ax2 = ax.twiny()
ax2.plot(kp0z/kp0, n_n0_depa)
ax2.set_xlabel(r'z [m] (assume $\lambda_{L0}=800\ {\rm nm}$)')
ax = axT[1]
ax.plot(kp0z, np.sqrt(k_kp0_depa/k_kp0_depa[0]))
ax.set_xlabel(r'$\omega_{p0}t=k_{p0}z$')
ax.set_ylabel(r'$k/k_0$')
ax2 = ax.twiny()
ax2.plot(kp0z/kp0, np.sqrt(k_kp0_depa/k_kp0_depa[0]))
ax2.set_xlabel(r'z [m] (assume $\lambda_{L0}=800\ {\rm nm}$)')
plt.tight_layout()
```

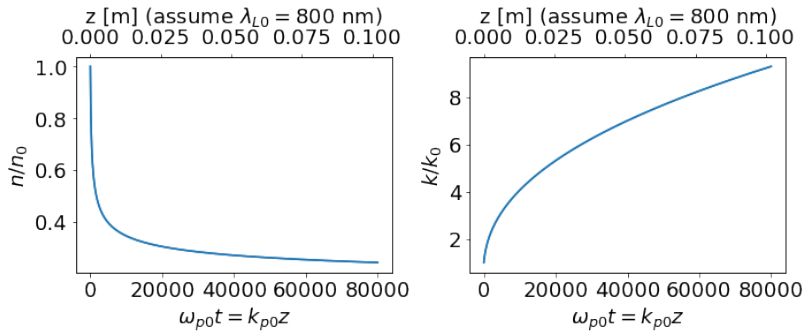

FIG. 5: Jupyter notebook output demonstrating usage of the Python code dephasingless_pwpa_plasma_profile to calculate the dephasingless PWPA plasma density profile and theoretical laser frequency.

```
In [6]: 1 help(depa.get_depa_profile)
```

```
Help on function get_depa_profile in module dephasingless_pwpa_plasma_profile:

get_depa_profile(nc0_np0, nd0_np0, kp0Ld0, n_n0_min=0.01, n_n0_max=1.1, kp0z_initial=0, kp0z_final=50000, n_steps=1
00001)
    Calculate the dephasingless plasma wakefield photon acceleration
    (dePWPA) plasma density profile and theoretical laser frequency

    Parameters
    ---
    nc0_np0: float, ratio of initial laser critical density to plasma density
    or ratio of laser frequency squared to plasma frequency squared
    nd0_np0: float, ratio of initial drive beam density to initial plasma density
    kp0Ld0: float, drive beam length normalized to initial plasma wavenumber
    n_n0_min: minimum possible plasma density ratio that can be computed
    n_n0_max: maximum possible plasma density ratio that can be computed
    kp0z_initial: float, start time/position of dePWPA profile
    kp0z_final: float, final time/position of dePWPA profile
    n_steps: number of integration steps in numerical solving of the dePWPA
    coupled differential equations

    Returns
    ---
    kp0z : numpy array
```

FIG. 6: A sample help message for the get_depa_profile function in the dephasingless_pwpa_plasma_profile Python code.

[1] J. Rossbach, J. R. Schneider, and W. Wurth, 10 years of pioneering x-ray science at the free-electron laser flash at desy, Physics Reports **808**, 1 (2019), 10 years of pioneering X-ray science at the Free-Electron Laser FLASH at DESY.

[2] M. A. Khokhlova and V. V. Strelkov, Highly efficient XUV generation via high-order frequency mixing, New Journal of Physics **22**, 093030 (2020).

[3] Z. Chang, A. Rundquist, H. Wang, M. M. Murnane, and H. C. Kapteyn, Generation of coherent soft x rays at 2.7 nm using high harmonics, Phys. Rev. Lett. **79**, 2967 (1997).

[4] S. V. Bulanov, T. Esirkepov, and T. Tajima, Light intensification towards the schwinger limit, Phys. Rev. Lett. **91**, 085001 (2003).

[5] M. Kando, A. S. Pirozhkov, K. Kawase, T. Z. Esirkepov, Y. Fukuda, H. Kiriyama, H. Okada, I. Daito, T. Kameshima, Y. Hayashi, H. Kotaki, M. Mori, J. K. Koga, H. Daido, A. Y. Faenov, T. Pikuz, J. Ma, L. M. Chen, E. N. Ragozin, T. Kawachi, Y. Kato, T. Tajima, and S. V. Bulanov, Enhancement of photon number reflected by the relativistic flying mirror, Phys. Rev. Lett. **103**, 235003 (2009).

[6] S. V. Bulanov, T. Z. Esirkepov, and M. Kando, Relativistic mirrors in plasmas. novel results and perspectives, Physics-Uspekhi **56**, 10.3367/UFNe.0183.201305a.0449 (2013).

[7] B. R. Benware, C. D. Macchietto, C. H. Moreno, and J. J. Rocca, Demonstration of a high average power tabletop soft x-ray laser, Phys. Rev. Lett. **81**, 5804 (1998).

[8] S. C. Wilks, J. M. Dawson, W. B. Mori, T. Katsouleas, and M. E. Jones, Photon accelerator, Physical Review Letters **62** (1989).

[9] J. T. Mendonca, Theory of photon acceleration (Institute of Physics Pub, 2001).

[10] W. Mori, The physics of the nonlinear optics of plasmas at relativistic intensities for short-pulse lasers, IEEE Journal of Quantum Electronics **33**, 1942 (1997).

[11] T. Esirkepov, S. V. Bulanov, M. Yamagiwa, and T. Tajima, Electron, positron, and photon wakefield acceleration: Trapping, wake overtaking, and ponderomotive acceleration, Physical Review Letters **96**, 014803 (2006).

[12] E. Esarey, G. Joyce, and P. Sprangle, Frequency upshifting of laser pulses by copropagating ionization fronts, Physical Review A **44**, 3908 (1991).

[13] L. Oliveira e Silva and J. T. Mendonca, Photon acceleration in superluminous and accelerated ionization fronts, IEEE Transactions on Plasma Science **24**, 316 (1996).

[14] M. R. Shcherbakov, K. Werner, Z. Fan, N. Talisa, E. Chowdhury, and G. Shvets, Photon acceleration and tunable broadband harmonics generation in nonlinear time-dependent metasurfaces, Nature Communications **10**, 1345 (2019).

[15] J. M. Dias, C. Stenz, N. Lopes, X. Badiche, F. Blasco, A. Dos Santos, L. Oliveira e Silva, A. Mysyrowicz, A. Antonetti, and J. T. Mendonça, Experimental evidence of photon acceleration of ultrashort laser pulses in relativistic ionization fronts, Phys. Rev. Lett. **78**, 4773 (1997).

[16] C. W. Siders, S. P. Le Blanc, D. Fisher, T. Tajima, M. C. Downer, A. Babine, A. Stepanov, and A. Sergeev, Laser wakefield excitation and measurement by femtosecond longitudinal interferometry, Phys. Rev. Lett. **76**, 3570 (1996).

[17] C. D. Murphy, R. Trines, J. Vieira, A. J. W. Reitsma, R. Bingham, J. L. Collier, E. J. Divall, P. S. Foster, C. J. Hooker, A. J. Langley, P. A. Norreys, R. A. Fonseca, F. Fiuza, L. O. Silva, J. T. Mendonça, W. B. Mori, J. G. Gallacher, R. Viskup, D. A. Jaroszynski, S. P. D. Mangles, A. G. R. Thomas, K. Krushelnick, and Z. Najmudin, Evidence of photon acceleration by laser wake fields, Physics of Plasmas **13**, 033108 (2006).

[18] M. R. Edwards, K. Qu, Q. Jia, J. M. Mikhailova, and N. J. Fisch, Cascaded chirped photon acceleration for efficient frequency conversion, Physics of Plasmas **25** (2018).

[19] Z. Nie, C. H. Pai, J. Hua, C. Zhang, Y. Wu, Y. Wan, F. Li, J. Zhang, Z. Cheng, Q. Su, S. Liu, Y. Ma, X. Ning, Y. He, W. Lu, H. H. Chu, J. Wang, W. B. Mori, and C. Joshi, Relativistic single-cycle tunable infrared pulses generated from a tailored plasma density structure, Nature Photonics **12**, 489 (2018).

[20] E. Esarey, A. Ting, and P. Sprangle, Frequency shifts induced in laser pulses by plasma waves, Physical Review A **42**, 3526 (1990).

[21] V. A. Mironov, A. M. Sergeev, E. V. Vanin, G. Brodin, and J. Lundberg, Upper limits for frequency upconversion in the nonlinear photon accelerator, Physical Review A **46**, R6178 (1992).

[22] S. V. Bulanov, V. I. Kirsanov, F. Pegoraro, and A. S. Sakharov, Charged particle and photon acceleration by wake field plasma waves in nonuniform plasmas, Laser Physics **3**, 1078 (1993).

[23] A. J. Howard, D. Turnbull, A. S. Davies, P. Franke, D. H. Froula, and J. P. Palastro, Photon Acceleration in a Flying Focus, Physical Review Letters **123**, 124801 (2019).

[24] J. P. Palastro, J. L. Shaw, P. Franke, D. Ramsey, T. T. Simpson, and D. H. Froula, Dephasingless laser wakefield acceleration, Phys. Rev. Lett. **124**, 134802 (2020).

[25] A. Debus, R. Pausch, A. Huebl, K. Steiniger, R. Widera, T. E. Cowan, U. Schramm, and M. Bussmann, Circumventing the Dephasing and Depletion Limits of Laser-Wakefield Acceleration, Physical Review X **9** (2019).

[26] C. Caizergues, S. Smartsev, V. Malka, and C. Thaury, Phase-locked laser-wakefield electron acceleration, Nature Photonics **14**, 475 (2020).

[27] S. V. Bulanov, V. A. Vshivkov, G. I. Dudnikova, N. M. Naumova, F. Pegoraro, and I. V. Pogorelsky, Laser acceleration of charged particles in inhomogeneous plasmas i, Plasma Physics Reports, **23**, 259 (1997).

[28] P. Sprangle, B. Hafizi, J. R. Peñano, R. F. Hubbard, A. Ting, C. I. Moore, D. F. Gordon, A. Zigler, D. Kaganovich, and T. M. Antonsen, Wakefield generation and GeV acceleration in tapered plasma channels, Physical Review E **63**, 056405 (2001).

[29] E. Guillaume, A. Döpp, C. Thaury, K. Ta Phuoc, A. Lifschitz, G. Grittani, J.-P. Goddet, A. Tafzi, S. Chou, L. Veisz, and V. Malka, Electron Rephasing in a Laser-Wakefield Accelerator, Physical Review Letters **115**, 155002 (2015).

[30] S. V. Bulanov, T. Z. Esirkepov, Y. Hayashi, H. Kiriyama, J. K. Koga, H. Kotaki, M. Mori, and M. Kando, On some theoretical problems of laser wake-field accelera-

tors, Journal of Plasma Physics **82**, 905820308 (2016).
[31] R. T. Sandberg and A. G. R. Thomas, Photon acceleration from optical to xuv, Phys. Rev. Lett. **130**, 10.1103/PhysRevLett.130.085001 (2023).
[32] J. B. Rosenzweig, Nonlinear plasma dynamics in the plasma wake-field accelerator, Physical Review Letters **58**, 555 (1987).
[33] S. Weinberg, Eikonal Method in Magnetohydrodynamics, Physical Review **126**, 1899 (1962).
[34] D. Guénot, D. Gustas, A. Vernier, B. Beaurepaire, F. Böhle, M. Bocoum, M. Lozano, A. Jullien, R. Lopez-Martens, A. Lifschitz, and J. Faure, Relativistic electron beams driven by kHz single-cycle light pulses, Nature Photonics **11**, 293 (2017).
[35] J. Kim, V. L. J. Phung, K. Roh, M. Kim, K. Kang, and H. Suk, Development of a density-tapered capillary gas cell for laser wakefield acceleration, Review of Scientific Instruments **92**, 023511 (2021).
[36] A. Akhiezer and R. Polovin, Theory of wave motion of an electron plasma, Journal of Experimental and Theoretical Physics **3**, 696 (1956).
[37] E. Infeld and G. Rowlands, Relativistic bursts, Physical Review Letters **62**, 10.1103/PhysRevLett.62.1122 (1989).
[38] P. Singh Verma, S. Sengupta, and P. Kaw, Bernstein-Greene-Kruskal waves in relativistic cold plasma, Physics of Plasmas **19**, 10.1063/1.3693357 (2012).
[39] P. S. Verma, S. Sengupta, and P. Kaw, Breaking of longitudinal Akhiezer-Polovin waves, Physical Review Letters **108**, 10.1103/PhysRevLett.108.125005 (2012).
[40] P. F. Byrd and M. D. Friedman, Handbook of Elliptic Integrals for Engineers and Scientists (Springer Berlin Heidelberg, Berlin, Heidelberg, 1971).
[41] T. P. Coffey, Breaking of Large Amplitude Plasma Oscillations, The Physics of Fluids **14**, 1402 (1971), https://pubs.aip.org/aip/pfl/article-pdf/14/7/1402/12445754/1402_1_online.pdf.
[42] J. B. Rosenzweig, B. Breizman, T. Katsouleas, and J. J. Su, Acceleration and focusing of electrons in two-dimensional nonlinear plasma wake fields, Phys. Rev. A **44**, R6189 (1991).
[43] A. Pukhov and J. Meyer-ter Vehn, Laser wake field acceleration: the highly non-linear broken- wave regime, Appl. Phys. B **74**, 355 (2002).
[44] W. Lu, C. Huang, M. Zhou, W. B. Mori, and T. Katsouleas, Nonlinear theory for relativistic plasma wakefields in the blowout regime, Phys. Rev. Lett. **96**, 165002 (2006).
[45] W. Lu, C. Huang, M. Zhou, et al., A nonlinear theory for multidimensional relativistic plasma wave wakefields, Phys. Plasmas **13**, 056709 (2006).
[46] A. Golovanov, I. Y. Kostyukov, A. Pukhov, and V. Malka, Energy-conserving theory of the blowout regime of plasma wakefield, Phys. Rev. Lett. **130**, 105001 (2023).
[47] A. Sainte-Marie, O. Gobert, and F. Quéré, Controlling the velocity of ultrashort light pulses in vacuum through spatio-temporal couplings, Optica **4**, 1298 (2017).
[48] D. H. Froula, D. Turnbull, A. S. Davies, T. J. Kessler, D. Haberberger, J. P. Palastro, S. W. Bahk, I. A. Begishev, R. Boni, S. Bucht, J. Katz, and J. L. Shaw, Spatiotemporal control of laser intensity, Nature Photonics **12**, 262 (2018).